Development of a Coupled Leaf and Canopy Model for the Simulation of Plant–Atmosphere Interaction

HONG-BING SU, KYAW THA PAW U, AND ROGER H. SHAW

Atmospheric Science, University of California, Davis, Davis, California

(Manuscript received 10 July 1995, in final form 6 November 1995)

ABSTRACT

A numerical scheme was developed to couple a multilayer canopy radiation model, a photosynthesis model for C_3 species, and a leaf stomatal conductance model with a single-leaf energy balance equation. This coupled leaf and canopy model was used to simulate the responses of a horizontally uniform forest canopy to its ambient microenvironment, using micrometeorological data collected from field measurements in a forest canopy. Emphasis was placed on issues associated with modeling the transient responses of plant leaves. For example, thermal storage was found to be important in modeling transience of leaf temperature, which in turn influenced the transient heating or cooling of the atmosphere by plant leaves. In addition, modification of the Ball–Berry leaf stomatal conductance model, using an exponential formula with an empirical time lag, yielded more realistic transient leaf stomatal conductances, which were important for estimating evaporation and CO_2 assimilation.

1. Introduction

Generally, factors controlling leaf stomatal responses to variations in the ambient environment can be partitioned into those that are closely associated with photosynthesis, such as net CO_2 assimilation, and others that are relatively independent of photosynthesis, such as wind speed, air temperature, and humidity (Wong et al. 1979; Ball and Berry 1982; Ball 1988).

Net absorbed solar and thermal radiation by plant leaves is important in determining leaf energy balance as well as photosynthesis. Therefore, a radiation model is needed to describe the radiative transfer within a plant canopy and to estimate absorbed solar and thermal radiation by plant leaves.

As part of an effort to develop a plant canopy model for linkage with a dynamic model of the atmospheric boundary layer turbulence, such as a higher-order closure model (Meyers and Paw U 1987; Paw U and Meyers 1989) or a large-eddy simulation (LES) (Shaw and Schumann 1992; Patton et al. 1995), we coupled a multilayer canopy radiation model, a leaf stomatal conductance model, and a photosynthesis model for leaves of C_3 species with a single-leaf energy balance equation. The primary goal was to simulate the responses of a plant canopy to its ambient microenvironment, which includes radiation, wind speed, ambient CO_2 concentration, air temperature, and humidity. Another goal was to assess the role of a plant canopy in the exchange of sensible heat, water vapor, and CO_2 with the ambient atmosphere.

In this paper, we first describe each leaf and canopy submodel. Second, we present analytical solutions for leaf stomatal conductance to water vapor, net CO_2 assimilation rate, and leaf temperature, as well as a numerical iteration scheme for solving the coupled system. Third, some sensitivity tests of our analytical solutions of leaf stomatal conductance and net CO_2 assimilation rate are presented. Finally, results are presented from simulations of the vertical and temporal variations of responses of a horizontally uniform forest canopy to its ambient atmosphere, using micrometeorological turbulence data from field measurements.

2. Descriptions of leaf and canopy submodels

a. Estimates of leaf boundary layer conductance

Leaf boundary layer conductance g_b, the reciprocal of leaf boundary layer resistance, depends upon the shape and size of a leaf and the Nusselt number (Nu). For heat transfer, Monteith (1973) gave

$$g_b = \frac{\mathrm{Nu}\nu_\theta}{D_L}, \tag{1}$$

where ν_θ is the thermal molecular diffusivity of air, and D_L is the characteristic dimension of an individual leaf.

For a flat plate under forced convection conditions, Nu is a function of the Reynolds number (Re) (Monteith 1973):

Corresponding author address: Hong-Bing Su, Atmospheric Science, Land, Air and Water Resources, University of California, Davis, Davis, CA 95616-8627.
E-mail: su@atm1.ucdavis.edu

$$\mathrm{Nu} = C_1\,\mathrm{Re}^{0.5}, \tag{2}$$

and

$$\mathrm{Re} = \frac{uD_L}{\nu}, \tag{3}$$

where ν is the kinematic molecular diffusivity of air, u is the wind speed, and C_1 is an empirical constant obtained from wind tunnel experiments.

In conditions of very light wind and significant leaf–air temperature difference, free convection becomes important. Under such conditions, Nu depends on the Grashof number (Gr) (Monteith 1973):

$$\mathrm{Nu} = C_2\,\mathrm{Gr}^{C_3}, \tag{4}$$

and

$$\mathrm{Gr} = \frac{g\beta_\theta D_L^3 |T_L - T_A|}{\nu^2}, \tag{5}$$

where β_θ is the volumetric expansion coefficient of air; g is gravitational acceleration; T_L and T_A are leaf and air temperature, respectively; and C_2 and C_3 are empirical constants obtained from experiments.

In this study, we have assumed that the leaf boundary layer conductances for the transfer of water vapor and CO_2 are the same as that for heat transfer. This is because the airflow within a plant canopy is usually highly turbulent (Jones 1992).

b. Leaf stomatal conductance model

The Ball–Berry model (Ball 1988) of leaf stomatal conductance to water vapor was employed:

$$g_{s,w} = m\frac{A_n}{c_s}\,\mathrm{rh}_s + b, \tag{6}$$

where $g_{s,w}$ (mol m^{-2} s^{-1}) is the leaf stomatal conductance to water vapor; A_n is the net CO_2 uptake rate at the leaf surface (mol m^{-2} s^{-1}); c_s (ppm) and rh_s are the CO_2 concentration and the fractional relative humidity at the leaf surface, respectively; and m and b are empirical regression coefficients determined from field and greenhouse experiments, which vary with species. When $A_n \leq 0$, $g_{s,w} = b$. In this study, we used $m = 9.29$ and $b = 0.008$ mol m^{-2} s^{-1}, which were obtained from gas-exchange experiments on *Glycine max* (Ball 1988). These values of m and b are typical of C_3 species, so we employed them as nominal values.

In this paper, we have used both meters per second (m s^{-1}) and moles per square meter per second (mol m^{-2} s^{-1}) as units of leaf conductance. For example, in the leaf stomatal conductance and photosynthesis models, we followed plant physiological convention and used the latter units. In the leaf energy balance equation and (40) and (41), we used meters per second. These stomatal conductances can be converted from one to the other using the universal gas law.

c. Photosynthesis model for leaves of C_3 species

The majority of crop and forest plants use the C_3 pathway in photosynthesis, including wheat, barley, potatos, sugar beets, beans, and trees (Jones 1992). Biochemical models of photosynthesis for leaves of C_3 species have been well studied and developed. The net CO_2 assimilation rate A_n for C_3 leaves has been expressed as (Farquhar et al. 1980)

$$A_n = V_c - 0.5V_o - R_d = \min(A_R, A_E) - R_d, \tag{7}$$

where V_c is the rate of carboxylation; V_o is the rate of oxygenation; R_d represents CO_2 evolution from mitochondria in the light that is sometimes termed "day respiration rate;" A_R is the Rubisco activity limit of CO_2 assimilation rate at lower intercellular CO_2 concentration when ribulose biphosphate (RuBP) is saturated; A_E is the CO_2 assimilation rate when the whole-chain electron transport limits RuBP regeneration; and the term $\min(A_R, A_E)$ represents the minimum of A_R and A_E.

Farquhar et al. (1980) expressed A_R as

$$A_R = V_{c\max}\frac{c_i - \Gamma_*}{c_i + K_c\left(1 + \dfrac{o_i}{K_o}\right)}, \tag{8}$$

where $V_{c\max}$ (mol m^{-2} s^{-1}) is the maximum catalytic activity of Rubisco at saturated RuBP and CO_2; c_i and o_i are the intercellular CO_2 and O_2 concentration, respectively; Γ_* is the CO_2 compensation point in the absence of mitochondrial or day respiration ($R_d = 0$); and K_c and K_o are the Michaelis constants for CO_2 and O_2, respectively.

Farquhar and von Caemmerer (1982) expressed A_E as

$$A_E = J\frac{c_i - \Gamma_*}{4.5c_i + 10.5\Gamma_*}, \tag{9}$$

where J (mol m^{-2} s^{-1}) is the potential rate of whole-chain electron transport.

As was the case in Leuning (1990), the smaller root of the following nonrectangular hyperbola equation was chosen as the solution of J:

$$\theta J^2 - (\alpha Q + J_{\max})J + \alpha Q J_{\max} = 0, \tag{10}$$

where $J_{\max}$ is the maximum rate of whole-chain electron transport at saturated light; Q is the absorbed photosynthetically active radiation (PAR) photon flux density (PFD) (mol m^{-2} s^{-1}); and α is the quantum efficiency. The curvature factor θ ($0 \leq \theta \leq 1$) determines how quickly the transition is made from the region of light-dependent maximum quantum yield to the light-

saturated rate. In this paper, we used $\alpha = 0.405$ (Ball 1988) and $\theta = 0.69$ (Evans and Farquhar 1991).

Moreover, R_d, V_{cmax}, Γ_*, J_{max}, K_c, and K_o depend on leaf temperatures, which need to be determined from experiments on various species. In this paper, we ignored the differences between various C_3 species and used leaf temperature dependencies of R_d and V_{cmax} given by Kirschbaum and Farquhar (1984) from greenhouse experiments using snow gum (*Eucalyptus pauciflora* Sieb. ex Spreng.), and that of Γ_* given by Brooks and Farquhar (1985) for intact spinach. Empirical formulas provided by Farquhar et al. (1980) and Farquhar (1988) from experiments using barley were employed for leaf temperature dependence of J_{max}. Arrhenius functions were used to estimate leaf temperature dependencies of K_c and K_o, as was done in Ball (1988) and Leuning (1990) for *Eucalyptus grandis*.

d. Leaf energy balance equation

An energy balance equation for a single leaf can be written as

$$\begin{aligned} R_{a,s} + R_{a,l} &= R_{e,l} + H + \mathrm{LE} + S \\ &= 2\epsilon_L \sigma T_L^4 + 2C_p \rho g_b (T_L - T_A) \\ &\quad + 2L_v \rho \frac{g_b g_{s,w}}{g_b + g_{s,w}} [q_s(T_L) - q_A] \\ &\quad + \rho_L C_L \left(\frac{V_L}{A_L}\right) \frac{\partial T_L}{\partial t}, \end{aligned} \quad (11)$$

where $R_{a,s}$ and $R_{a,l}$ are absorbed shortwave and longwave radiation, respectively; $R_{e,l}$ is emitted longwave radiation; H and LE are sensible and latent heat fluxes, respectively; S is physical storage; σ is the Stefan–Boltzmann constant; ϵ_L is thermal emissivity of the leaf; T_L is leaf temperature; ρ and C_p are air density and specific heat of air at constant pressure, respectively; g_b is leaf boundary layer conductance, which is assumed to be the same for heat, water vapor, and CO_2; T_A is air temperature; L_v is latent heat of vaporization; $g_{s,w}$ is leaf stomatal conductance to water vapor; $q_s(T_L)$ is the saturated water vapor mixing ratio at leaf temperature; q_A is the mixing ratio of water vapor in the air; ρ_L and C_L are density and specific heat of leaf, respectively; V_L and A_L are the volume and surface area of a leaf, respectively; and $\partial T_L/\partial t$ represents the time derivative of leaf temperature. The ratio of V_L/A_L depends upon the shape of a plant leaf. For a broad flat leaf, it is equal to the leaf thickness.

e. Multilayer canopy radiation model

For a horizontally homogeneous canopy, only the vertical distributions of absorbed shortwave and longwave radiation by plant leaves need to be calculated to solve the leaf energy balance and leaf photosynthesis.

A one-dimensional multilayer (20-layer canopy with equal intervals in the vertical direction) radiative transfer model based on the work of Norman (1979) and modified by Paw U and Meyers (1989) was adopted here. The PAR and near-infrared radiation (NIR) of solar radiation as well as thermal radiation (IR) were treated separately because leaf spectral properties are quite different for PAR, NIR, and IR. Incoming solar radiation was also partitioned into direct-beam and diffuse components because the penetration of direct-beam radiation and diffuse radiation through a plant canopy are quite different (Weiss and Norman 1985). The spherical distribution of leaf inclination has been widely used (Norman 1979) because plant leaves usually do not have a predominant angle. A recent study (Baldocchi 1994b) has shown the effects of clumped leaves on the computation of radiative transfer within crop and forest canopies. In this study, we modeled a sparse forest canopy (LAI = 2), in which leaves are not greatly clumped. Therefore, the simpler spherical leaf inclination distribution was adopted, with equal leaf angle intervals between 0 and $\pi/2$ representing nine classes of leaf angle. Photosynthesis, stomatal conductance, and leaf energy balance could be very different for sunlit leaves than for shaded leaves. Therefore, an estimate of the fraction of sunlit leaves was needed. We used the formula provided by Norman (1979) to calculate the fraction of sunlit leaf area in each layer of a plant canopy for a spherical leaf angle distribution.

3. Coupling processes of leaf and canopy models

a. The quadratic equation for stomatal conductance $g_{s,w}$

In order to use the Ball–Berry formula (6) to estimate leaf stomatal conductance to water vapor, one must estimate the fractional relative humidity rh_s and CO_2 concentration at the leaf surface c_s. These can be expressed as follows:

$$\mathrm{rh}_s = \frac{g_b q_A + g_{s,w} q_s(T_L)}{(g_b + g_{s,w}) q_s(T_L)}, \quad (12)$$

and

$$c_s = c_A - \frac{A_n}{g_b}. \quad (13)$$

The above two equations were combined with the Ball–Berry formula (6) to obtain a quadratic equation with the limitation of $A_n > 0$, with respect to $g_{s,w}$.

$$A_g g_{s,w}^2 + B_g g_{s,w} + C_g = 0, \quad (14)$$

where

$$A_g = c_s = c_A - \frac{A_n}{g_b}, \quad (15)$$

$$B_g = \left(c_A - \frac{A_n}{g_b}\right)(g_b - b) - mA_n, \quad (16)$$

and

$$C_g = -g_b b\left(c_A - \frac{A_n}{g_b}\right) - mA_n g_b \frac{q_A}{q_s(T_L)}. \quad (17)$$

Parameter C_g is usually less than zero because g_b, b, m, q_A, and $q_s(T_L)$ are greater than zero, and c_s is also greater than zero. Therefore, the above quadratic equation usually yields one positive and one negative real solution, with the positive solution being physically reasonable. This has been confirmed by our preliminary tests of the above solution for a wide range of A_n, g_b, and q_A, as shown later.

b. The cubic equation for net CO_2 assimilation rate A_n

A cubic equation with respect to A_n can be derived as follows, similar to Baldocchi's derivation (1994a). First, substitute (13) into (6) to eliminate c_s. Then, eliminate $g_{s,w}$ by substituting (6) into the intercellular CO_2 concentration c_i equation

$$c_i = c_A - A_n \frac{g_{s,w} + g_b\gamma_{w,c}}{g_{s,w}g_b}, \quad (18)$$

where $\gamma_{w,c} \approx 1.647$ is the ratio of molecular diffusivity of water vapor to that of CO_2.

According to (8) and (9), a general algebraic form of A_n can be written as

$$A_n = a_A \frac{c_i - \Gamma_*}{e_A c_i + d_A} - R_d. \quad (19)$$

Insert (18) into (19) to eliminate c_i and obtain a cubic equation with respect to A_n.

$$C_{A,3}A_n^3 + C_{A,2}A_n^2 + C_{A,1}A_n + C_{A,0} = 0, \quad (20)$$

where

$$C_{A,3} = e_A\alpha_A, \quad (21)$$

$$C_{A,2} = e_A\beta_A + d_A\theta_A + (e_A R_d - a_A)\alpha_A, \quad (22)$$

$$C_{A,1} = \left(e_A + \frac{d_A}{c_A}\right)\gamma_A + R_d(e_A\beta_A + d_A\theta_A) + a_A(\Gamma_*\theta_A - \beta_A), \quad (23)$$

$$C_{A,0} = \gamma_A\left[a_A\left(\frac{\Gamma_*}{c_A} - 1\right) + R_d\left(e_A + \frac{d_A}{c_A}\right)\right], \quad (24)$$

and

$$\alpha_A = \gamma_{w,c} + \frac{b}{g_b} - m\mathrm{rh}_s, \quad (25)$$

$$\beta_A = c_A[g_b(m\mathrm{rh}_s - \gamma_{w,c}) - 2b], \quad (26)$$

$$\theta_A = g_b m\mathrm{rh}_s - b, \quad (27)$$

$$\gamma_A = c_A^2 b g_b. \quad (28)$$

Tests with a wide range of values of PAR, T_L, c_A, rh_s, and g_b showed that there are three different real roots of cubic equation (20). However, the following root has always been the only physiologically and physically possible solution for A_n.

$$A_n = 2r_A^{1/3}\cos\left(\Theta + \frac{4\pi}{3}\right) - \frac{C_{A,2}}{3C_{A,3}}, \quad (29)$$

where

$$r_A = \left[\left(\frac{C_{A,2}}{3C_{A,3}}\right)^2 - \frac{C_{A,1}}{3C_{A,3}}\right]^{3/2}, \quad (30)$$

and

$$\Theta = \frac{1}{3}\cos^{-1}\left[-\frac{\frac{C_{A,0}}{C_{A,3}} - \frac{C_{A,1}C_{A,2}}{3C_{A,3}^2} + \frac{2C_{A,2}^3}{27C_{A,3}^3}}{2r_A}\right]. \quad (31)$$

c. The quartic equation for leaf temperature T_L

In the leaf energy balance equation (11), $R_{a,s}$ and $R_{a,l}$ are determined from the canopy radiation model, g_b is estimated from (1)–(5), and $g_{s,w}$ is determined by solving (14). Other inputs include T_A and q_A. Then, using the fourth-order polynomial for the saturated vapor pressure and (11), a quartic equation with respect to leaf temperature T_L can be derived (Paw U 1987).

$$C_{T,4}T_L^4 + C_{T,3}T_L^3 + C_{T,2}T_L^2 + C_{T,1}T_L + C_{T,0} = 0, \quad (32)$$

where

$$C_{T,4} = 2\sigma\epsilon_L + 2L_v\rho g_{t,w}\frac{C_{e,4}\epsilon}{P}, \quad (33)$$

$$C_{T,3} = 8\sigma\epsilon_L T_0 + 2L_v\rho g_{t,w}\frac{C_{e,3}\epsilon}{P}, \quad (34)$$

$$C_{T,2} = 12\sigma\epsilon_L T_0^2 + 2L_v\rho g_{t,w}\frac{C_{e,2}\epsilon}{P}, \quad (35)$$

$$C_{T,1} = 8\sigma\epsilon_L T_0^3 + 2C_p\rho g_b + 2L_v\rho g_{t,w}\frac{C_{e,1}\epsilon}{P} + C_{T,S}, \quad (36)$$

and

$$C_{T,0} = 2\sigma\epsilon_L T_0^4 - 2C_p\rho g_b T_A + 2L_v\rho g_{t,w}\left(\frac{C_{e,0}\epsilon}{P} - q_A\right) - R_{a,s} - R_{a,l} - C_{T,S}T_{L,o}. \quad (37)$$

Here, $C_{e,0} = 617.4$ Pa, $C_{e,1} = 42.22$ Pa °C^{-1}, $C_{e,2}$

$= 1.675$ Pa °C^{-2}, $C_{e,3} = 1.408 \times 10^{-2}$ Pa °C^{-3}, and $C_{e,4} = 5.818 \times 10^{-4}$ Pa °C^{-4}; $\epsilon = 0.622$ is the ratio of molecular weight of water vapor to that of dry air; $P = 101\ 325$ Pa is the total air pressure, and

$$g_{t,w} = \frac{g_b g_{s,w}}{g_b + g_{s,w}}, \tag{38}$$

$$C_{T,S} = \frac{\rho_L C_L (V_L/A_L)}{\Delta t}, \tag{39}$$

and $T_0 = 273.15$ K; $g_{t,w}$ is overall leaf conductance to evaporation; Δt is the time interval between time steps at which leaf temperature is calculated; T_L is the leaf temperature at the present time; and $T_{L,O}$ is that at the former time step. The last term in (36) and that in (37) are ignored if the physical storage term in (11) is neglected.

Paw U (1987) pointed out that of the four roots of (32), two are complex, one is physically nonsensical, and one is realistic. Moreover, the fact that the same root is always the realistic value was confirmed by our tests over a wide range of values of air temperature, humidity, leaf boundary layer and stomatal conductances, radiation, etc.

d. Coupling process of leaf and canopy models

All leaf and canopy models employed here are steady state and nonlinearly depend on each other either explicitly or implicitly. For example, leaf stomatal conductance $g_{s,w}$ explicitly depends upon net CO_2 assimilation rate A_n, which depends upon leaf temperature T_L and relative humidity at the leaf surface rh_s. However, rh_s also depends upon $g_{s,w}$, and T_L, which is solved from the leaf energy balance equation. In addition, $g_{s,w}$ is needed in solving T_L. Finally, emission of thermal radiation by plant leaves depends upon leaf temperature as well.

A numerical iteration scheme for solving the above coupled leaf and canopy system is shown in Fig. 1. First, as part of the initial conditions, absorbed total shortwave radiation $R_{a,s}$ and PAR PFD by both sunlit and shaded leaves, as well as the fraction of sunlit leaves, are calculated separately by the canopy radiation model. The shortwave radiation $R_{a,s}$ and PAR PFD can be updated whenever necessary. Other initial conditions include wind speed u, ambient CO_2 concentration c_A, air temperature T_A, and water vapor mixing ratio q_A. Following this, the initial value of absorbed thermal radiation $R_{a,l}$ is estimated by the canopy thermal radiation model, which is assumed to be the same for both sunlit and shaded leaves. Third, sunlit and shaded leaves are separated into iteration loops to solve for net CO_2 assimilation rate A_n, leaf stomatal conductance to water vapor $g_{s,w}$, and leaf temperature T_L. Then, the mean leaf temperature is calculated from the weighted average of the fourth power of leaf temperature of sunlit leaves and that of shaded leaves. Finally, absorbed thermal radiation $R_{a,l}$ by plant leaves is updated using the new mean leaf temperature. Convergence criteria are 1×10^{-12} mol m^{-2} s^{-1} for A_n, 1×10^{-13} mol m^{-2} s^{-1} for $g_{s,w}$, 1×10^{-8} for rh_s, 1×10^{-3} °C for T_L, and 1×10^{-2} W m^{-2} for $R_{a,l}$. The convergence of the fractional relative humidity at leaf surface rh_s was added because rh_s is needed in solving for A_n and is updated after each new estimate of $g_{s,w}$. Using the above criteria, only a few iteration steps are needed to reach numerical convergence. Tests using more stringent convergence criteria and more iteration steps demonstrated that the above criteria are adequate.

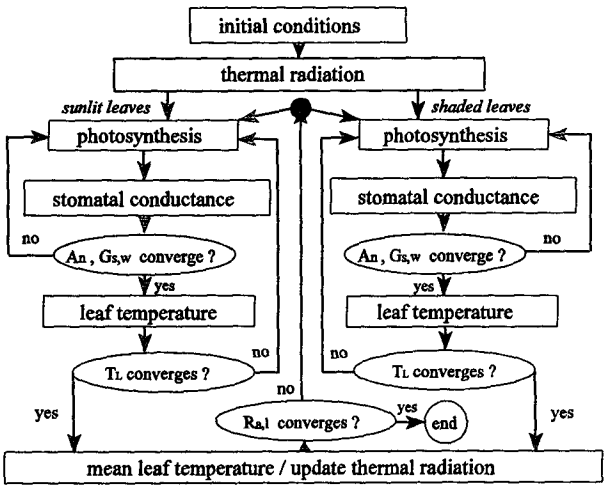

FIG. 1. Flowchart of a numerical iteration scheme for solving a coupled photosynthesis model, a leaf stomatal conductance model, a leaf energy balance equation, and a canopy thermal radiation model.

e. Model applications

1) RATES OF HEATING, EVAPORATION, AND CO_2 REDUCTION BY PLANT LEAVES

The subgrid volume-averaged rates of sensible heat, water vapor, and CO_2 exchange between plant leaves and the ambient atmosphere, which are represented by S_θ(°C s^{-1}), S_q(g kg^{-1} s^{-1}), and S_C (ppm s^{-1}), respectively, can be defined as follows:

$$S_\theta = 2a_L g_b (T_L - T_A), \tag{40}$$

$$S_q = 2a_L \frac{g_b g_{s,w}}{g_b + g_{s,w}} [q_s(T_L) - q_A], \tag{41}$$

and

$$S_C = 2a_L A_n, \tag{42}$$

where a_L is the leaf area density, which is defined as the total area (one-sided only) of leaves per unit volume. For a horizontally uniform canopy divided into a

number of layers, S_θ, S_q, S_C, T_L, T_A, $q_s(T_L)$, q_A, A_n, a_L, g_b, and $g_{s,w}$ are corresponding mean values for each layer of the canopy.

2) Spatial variations

We simulated a horizontally uniform forest canopy under steady-state conditions. The height of this forest was set to 20 m and the forest was divided into 20 layers with an equal interval of 1 m. The vertical profile of leaf area density was assumed to be similar to that used by Shaw and Schumann (1992), with the leaf area index LAI = 2, as shown in Fig. 2. The solar zenith angle and total solar radiation reaching the top of the forest were set to 10° and 900 W m^{-2}, respectively. The mean wind profile within the forest was specified as shown in Fig. 3, with a shape similar to those obtained in real forest canopies (Kaimal and Finnigan 1994). Vertical profiles of air temperature, water vapor mixing ratio, and ambient CO_2 concentration were specified as shown in Fig. 9a, Fig. 9b, and Fig. 3, respectively, which were similar to those obtained from a real 20-m forest over a period of one hour near noon (Denmead and Bradley 1985).

3) Temporal (transient) variations

As reported by Jones (1992), early studies in transient stomatal response have shown that stomatal opening and closing are very sensitive to light intensity and that closing tends to be more rapid than opening, with a timescale on the order of 2–5 min. Moreover, stomata tend to open as leaf temperature increases and close in response to increased leaf–air humidity difference. For apple trees, it was reported that 90% of the total stomatal closing response to an increase in leaf–air vapor pressure difference occurred within 20 s, while opening responses tend to be somewhat slower (Fanjul and Jones 1982).

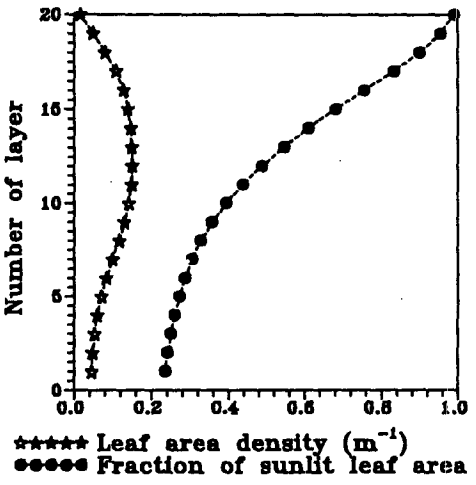

FIG. 2. Vertical profiles of leaf area density (LAI = 2) and fraction of sunlit leaf area (solar zenith angle 10°).

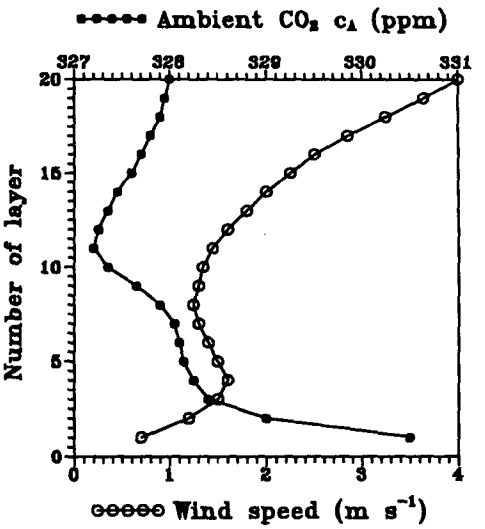

FIG. 3. Vertical profiles of mean wind speed and CO_2 concentration within a model forest.

As an approximation to describe stomatal time response, we used the exponential function

$$g_{s,w}(t_n) = g_{s,w}(t_{n-1}) + [g^*_{s,w}(t_n) - g_{s,w}(t_{n-1})] \times \left[1 - \exp\left(-\frac{t_n - t_{n-1}}{\tau_s}\right)\right], \quad (43)$$

where $g^*_{s,w}(t_n)$ is the calculated Ball–Berry stomatal conductance to water vapor at time step t_n; $g_{s,w}(t_n)$ and $g_{s,w}(t_{n-1})$ are leaf stomatal conductance to water vapor at time steps t_n and t_{n-1}, respectively; and τ_s is a time constant for stomatal response. In this preliminary study, we have assumed the same time constant, τ_s = 20 s, for both stomatal opening and closing.

Experiments have shown that turbulent time series of air temperature and humidity within and above a plant canopy often include ramp patterns with a slow increase or decrease in air temperature and humidity for tens of seconds, terminated by a very sharp drop or rise lasting a few seconds. The drop is typically a few degrees Celsius in temperature and a few grams per kilogram in mixing ratio (Gao et al. 1989; Shaw et al. 1989; Paw U et al. 1992). These ramp structures are associated with so-called coherent structures in the turbulent flow composed of combined ejection and sweep motions. Therefore, it is important for us to test how our model describes transient behavior of leaf temperature as well as leaf stomatal conductance, which are usually believed to vary much more slowly than wind speed, air temperature, and humidity.

We used 30 min of turbulent wind velocity, air temperature, and humidity data from a field experiment that

was performed at a deciduous forest site at Camp Borden, Ontario, Canada during the fall of 1986 (Shaw et al. 1988). The original 10-Hz data were resampled as turbulent fluctuations from the means and block averaged to obtain 1-Hz data. The turbulent fluctuations of wind speed, air temperature, and humidity were linearly interpolated or extrapolated to all levels in our model and then added to the mean profiles described earlier to obtain time series. Figure 4 shows the measured time series of air temperature, mixing ratio, and wind speed for about 14 min of the half-hour period at the top of the forest. These data exhibited well-defined ramp structures repeated in both air temperature and water vapor mixing ratio, as well as a repeated gust signal in the wind speed.

For the leaf energy balance equation with thermal storage [Eq. (11)], we assumed the total shortwave radiation and PAR absorbed by both sunlit leaves and shaded leaves were constant during the 30-min period and ignored the occurrence of moving sunflecks. In addition, the CO_2 concentration profile within the forest was also assumed to be constant with time because 10-Hz data were not available.

4. Sensitivity tests of the analytical solutions for A_n and $g_{s,w}$

a. The net CO_2 assimilation rate A_n

From sections 2c and 3b, we know that the analytical solution for A_n explicitly depends upon the PAR PFD, ambient CO_2 concentration c_A, leaf boundary layer conductance g_b, and relative humidity at the leaf surface rh_s, as well as other parameters that are either constant or only dependent on leaf temperature T_L. The dependence of net CO_2 assimilation rate A_n on PFD and c_A is well known (Farquhar and von Caemmerer 1982; Baldocchi 1994a). For the sake of brevity, we only show the dependence of A_n on g_b because of the direct linkage between g_b and the wind speed, which varies both in time and space in a plant canopy. Figure 5 shows that A_n increases with increasing g_b until the PAR absorbed by plant leaves becomes the dominant limit of CO_2 assimilation. In addition, when the wind is very light, g_b becomes the important limit of CO_2 assimilation.

b. The leaf stomatal conductance to water vapor $g_{s,w}$

The analytical solution of $g_{s,w}$ explicitly depends upon net CO_2 assimilation rate A_n, ambient CO_2 concentration c_A, mixing ratio in ambient air q_A, saturated mixing ratio at leaf temperature $q_s(T_L)$, and leaf boundary layer conductance g_b (sections 2b and 3a). For the sake of brevity, only the dependencies of $g_{s,w}$ on A_n and q_A are shown. Figure 6 shows that $g_{s,w}$ increases nonlinearly with increasing q_A and A_n, and this nonlinearity increases when q_A decreases for given c_A and g_b, especially for extremely dry air (very small q_A).

5. Results of model applications

a. Spatial variations

A vertical profile of the fraction of sunlit leaf area was calculated from the canopy radiation model (shown in Fig. 2). Figure 7 shows vertical profiles of net PAR, NIR, and total shortwave and longwave radiation within the forest, which were also calculated from the canopy radiation model. PAR, shortwave gain, and longwave loss are greater in the upper half of the modeled forest than in the lower half.

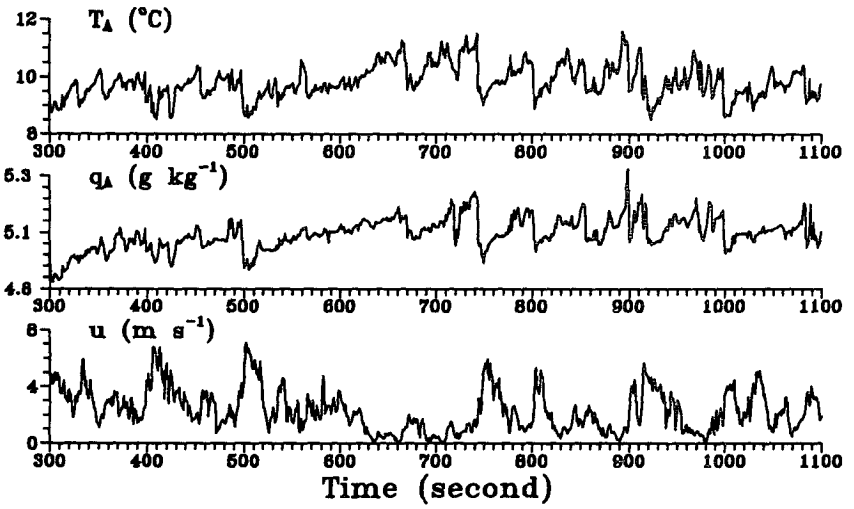

FIG. 4. Time series of measured wind speed u, air temperature T_A, and water vapor mixing ratio q_A at the top of Borden forest.

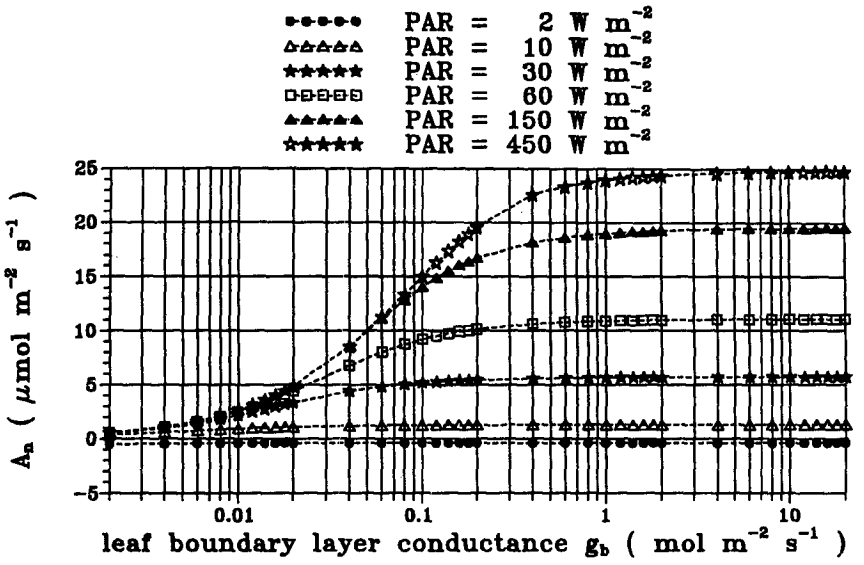

FIG. 5. The g_b dependence of A_n at various PAR when c_A = 350 ppm, leaf temperature T_L = 25°C, and rh_s = 0.85.

Figure 8 shows that the longwave radiation losses for both sunlit and shaded leaves are larger in the upper half of the modeled forest than in the lower half. Shortwave radiation absorbed by shaded leaves, which decreases from the top to the bottom of the forest, is much less than that absorbed by sunlit leaves, which is quite constant through the whole canopy. The latent heat from sunlit leaves is much greater than that from shaded leaves through the canopy, neither of which vary very much in the vertical. This is because leaf stomatal conductance is larger for sunlit leaves than that for shaded leaves, and both are smaller than leaf boundary layer conductance. In this case, the leaf–air humidity difference is greater for sunlit leaves than for

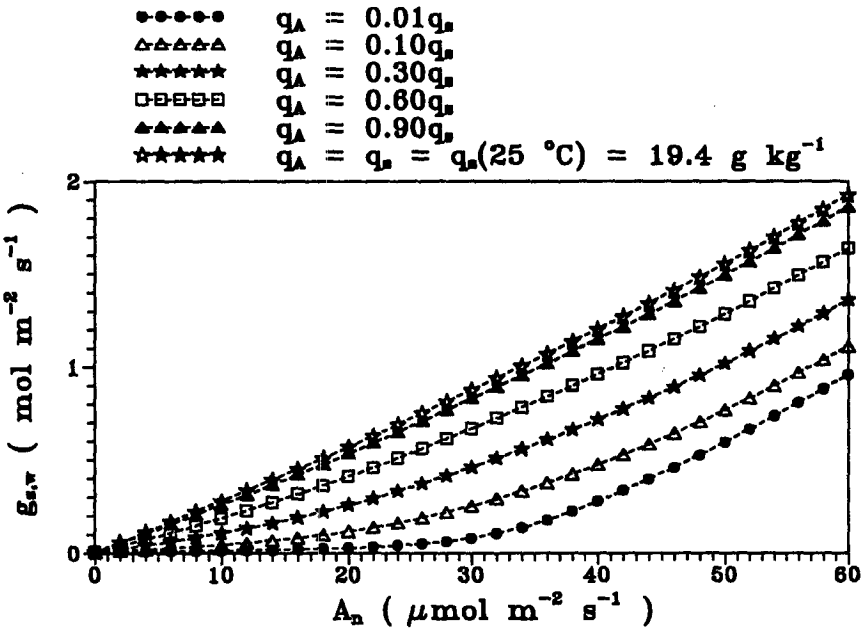

FIG. 6. The A_n dependence of $g_{s,w}$ at various q_A when T_L = 25°C, $q_s(T_L)$ ≈ 19.4 g kg^{-1}, c_A = 350 ppm, and g_b = 1 mol m^{-2} s^{-1}.

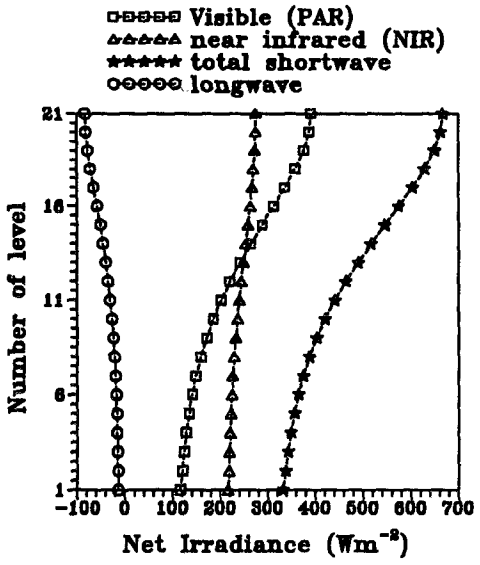

FIG. 7. Profiles of net irradiances within the model forest.

shaded leaves (Fig. 9b). Sunlit leaves are heating the air, while shaded leaves are cooling the air. The residual, defined as the total absorbed shortwave and longwave radiation by a leaf minus the sensible heat, latent heat, and thermal radiation emitted by the leaf, is very small, which demonstrates that our solution of the leaf energy balance equation is numerically valid.

Figure 9a shows that heating by sunlit leaves reaches a maximum near the top of the canopy, while maximum cooling by shaded leaves appears near the middle of the canopy. As we know, the profile of subgrid volume-averaged heating or cooling rate S_θ is determined by the combination of profiles of leaf boundary layer conductance (Fig. 8), leaf–air temperature difference (Fig. 9a), and fraction of sunlit leaf area (Fig. 2). For example, leaf–air temperature difference for sunlit leaves reaches a maximum at the bottom of canopy; however, heating by sunlit leaves is at a minimum because leaf boundary layer conductance is at a minimum, and there are few sunlit leaves there. Overall, in the modeled case, plant leaves are heating ambient air in the upper one-third of the canopy while cooling the air in the lower two-thirds. The difference between mean leaf temperature (calculated from the weighted average of the fourth power of sunlit and shaded leaf temperature) and air temperature corresponds very well to the overall heating or cooling (Fig. 9a).

In addition, the overall evaporation (S_q) and CO_2 assimilation (S_C) appear mostly in the upper half of the forest (Fig. 9b,c) where there are the most leaves. Evaporation from sunlit leaves is much greater than that from shaded leaves, especially in the upper half of the canopy. Assimilation of CO_2 by sunlit leaves is greater than that by shaded leaves in the upper half of the forest, but this reverses in the lower half. The net CO_2 assimilation rate at individual leaf surface A_n for shaded leaves, which decreases from the top to the bottom of the canopy, is much less than that for sunlit leaves, which is more constant throughout the whole canopy.

b. Temporal (transient) variations

Figure 10 shows that leaf temperature T_L responds instantly to air temperature T_A if the thermal storage is excluded. In addition, T_L increases sharply when the wind is very light and evaporative cooling of leaves is strongly limited, as indicated by the arrows in Fig. 10. When the thermal storage is included, the sharp increase in leaf temperature T_L disappears, there is a time lag of approximately 10 s for a 0.1-mm-thick leaf, and the amplitude of the variations is attenuated. Thicker leaves (0.3 mm) have a larger time lag and smaller amplitude of leaf temperature variations than thinner leaves, as expected. Although high-frequency data on leaf temperature were not available for the Borden experiment, they were taken over maize canopies (Paw U et al. 1992), where the data showed traces similar to the thermal storage traces in Fig. 10.

As noted earlier, when the wind is extremely light, the leaf boundary layer conductance g_b becomes the dominant limiting factor of evaporation, as shown by the arrows in the time traces of total conductance to water vapor $g_{t,w}$ and subgrid volume-averaged evaporation rate S_q (Fig. 10).

The leaf stomatal conductance to water vapor $g_{s,w}$ shows unrealistically high-frequency variations when the stomatal response is considered instantaneous (Fig. 11). The leaf stomatal conductance $g_{s,w}$ varies much more smoothly when (43) is used to introduce a time lag in stomatal response. In addition, the transient evaporation rate S_q becomes smoother and smaller than that for instantaneous stomatal response (Fig. 10).

The transient subgrid volume-averaged heating rate S_θ has much greater temporal variation when the thermal storage is included (Fig. 12). This is expected because leaf temperature follows air temperature quickly and temporal variations of leaf–air temperature difference are very small, if the thermal storage is excluded. The peaks in the S_θ trace correspond to either gusts in wind speed or the sharp drop in air temperature T_A as indicated by the arrows in Fig. 12. The correlation coefficient between u and S_θ is 0.78 for the 30-min period modeled in this study. This can be explained by (40) and the direct linkage between leaf boundary layer conductance g_b and wind speed u.

However, the bottom graph in Fig. 12 shows that the difference between the normalized vertical eddy-covariance heat flux and the normalized subgrid volume-averaged sensible heating rate by plant leaves S_θ is much greater during gusts than during more quiescent

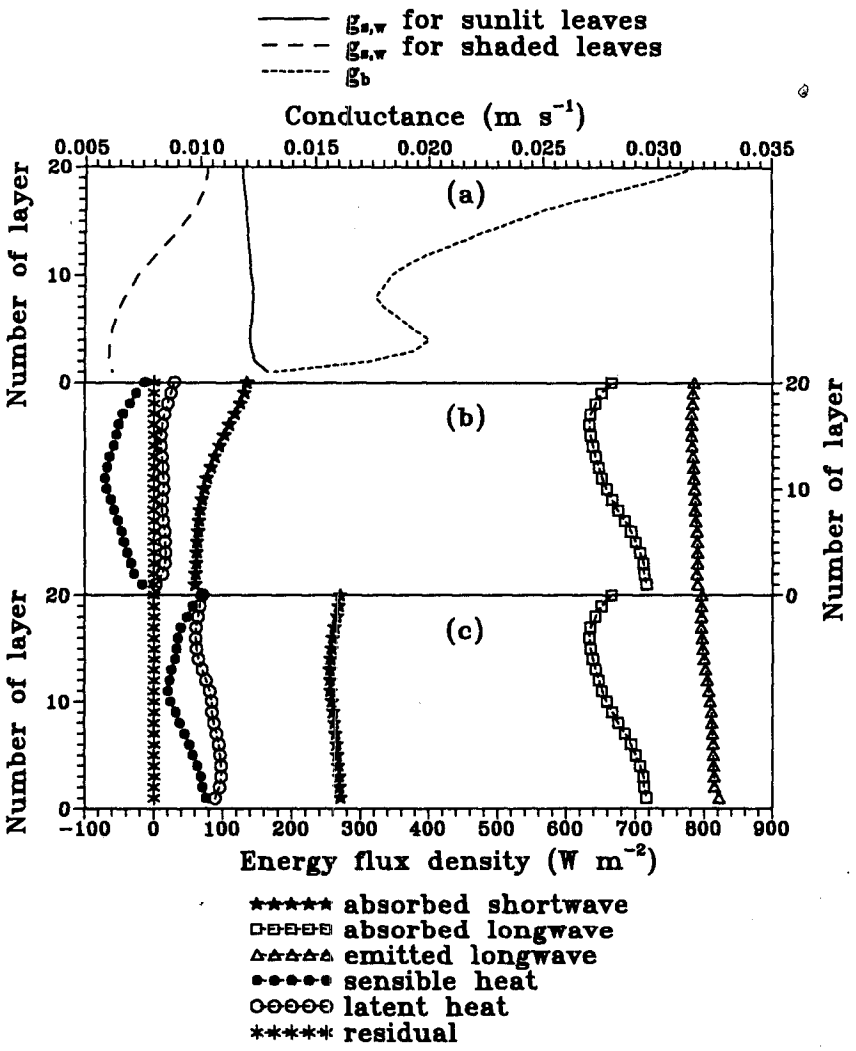

FIG. 8. Profiles of g_b and $g_{s,w}$ (a); and energy balance for individual (b) shaded and (c) sunlit leaves.

periods. Peaks in the normalized eddy-covariance heat flux frequently do not coincide with the peaks in S_θ traces, especially during some gust periods. The correlation coefficient between them is only 0.28 for the 30-min period modeled in this study, which implies that the instantaneous or short-time-averaged eddy-covariance heat flux may not be an accurate depiction of transient subgrid volume-averaged sensible heat exchange between plant leaves and the air. This is because of the strong short-time advection during the gusts (coherent structures) and the nonlocal (large scale) turbulent transport of heat.

In addition, the bottom graph in Fig. 12 shows that the vertical eddy-covariance heat flux is much more intermittent than the subgrid volume-averaged heating rate S_θ. This is because the large eddies (coherent structures) contribute a great portion of the eddy-covariance heat flux and are strongly intermittent. On the other hand, the sensible heat exchange between plant leaves and the ambient air is accomplished by much smaller eddies, with scales limited by the thickness of the leaf boundary layer and the characteristic dimension of leaves.

The time traces of CO_2 concentration in the intercellular space c_i and at the leaf surface c_s exhibit sharp drops when the wind is extremely light and CO_2 cannot be transported to the leaf surface and the intercellular space efficiently (Fig. 13). The subgrid volume-averaged CO_2 assimilation rate S_C varies more smoothly than S_θ (sensible heat) and S_q (evaporation). There are two main factors responsible for this difference. First, the ambient CO_2 was assumed to be constant with time (measurements were not taken), while the ambient air temperature and humidity varied with time. Second, the

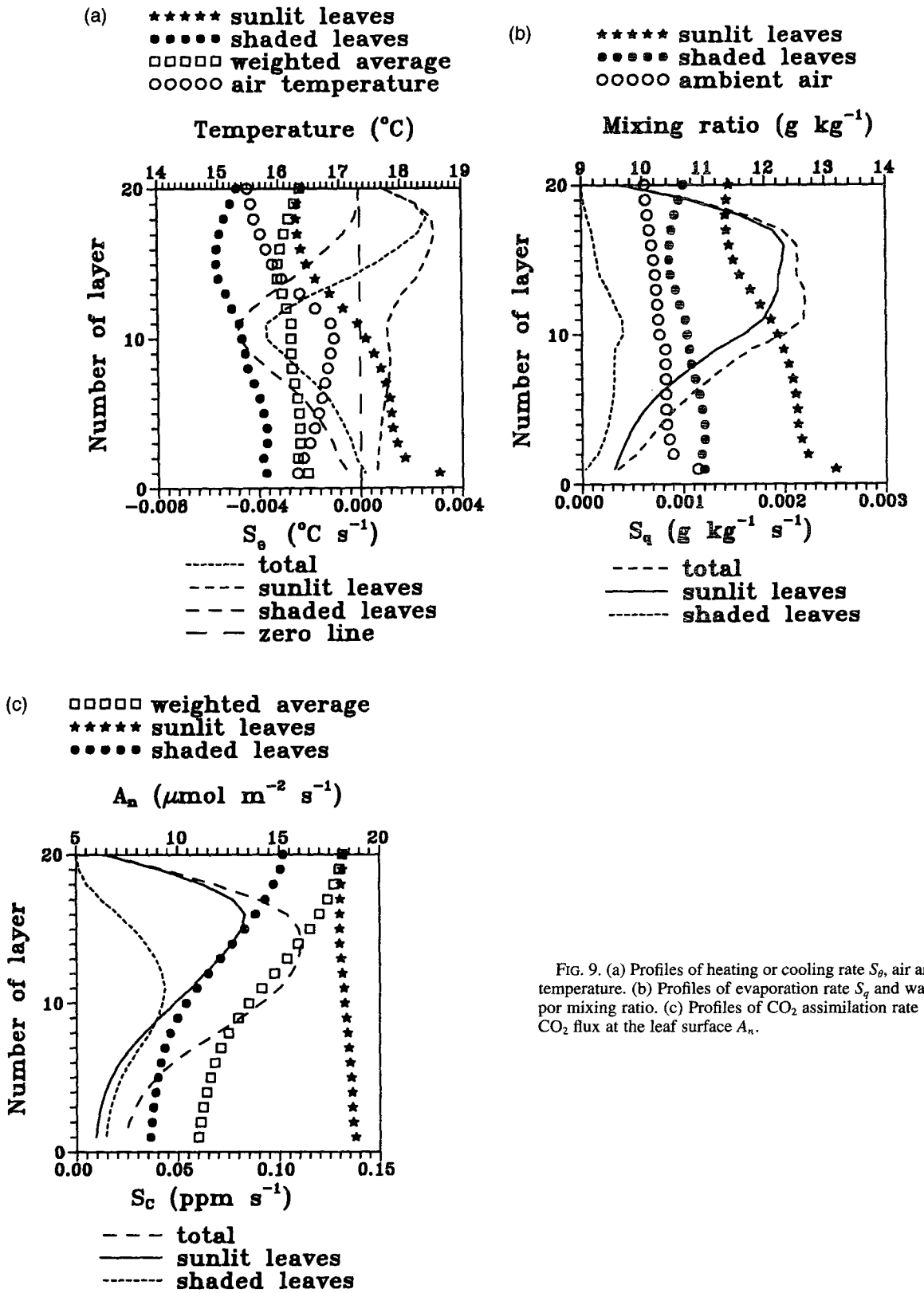

FIG. 9. (a) Profiles of heating or cooling rate S_θ, air and leaf temperature. (b) Profiles of evaporation rate S_q and water vapor mixing ratio. (c) Profiles of CO_2 assimilation rate S_C and CO_2 flux at the leaf surface A_n.

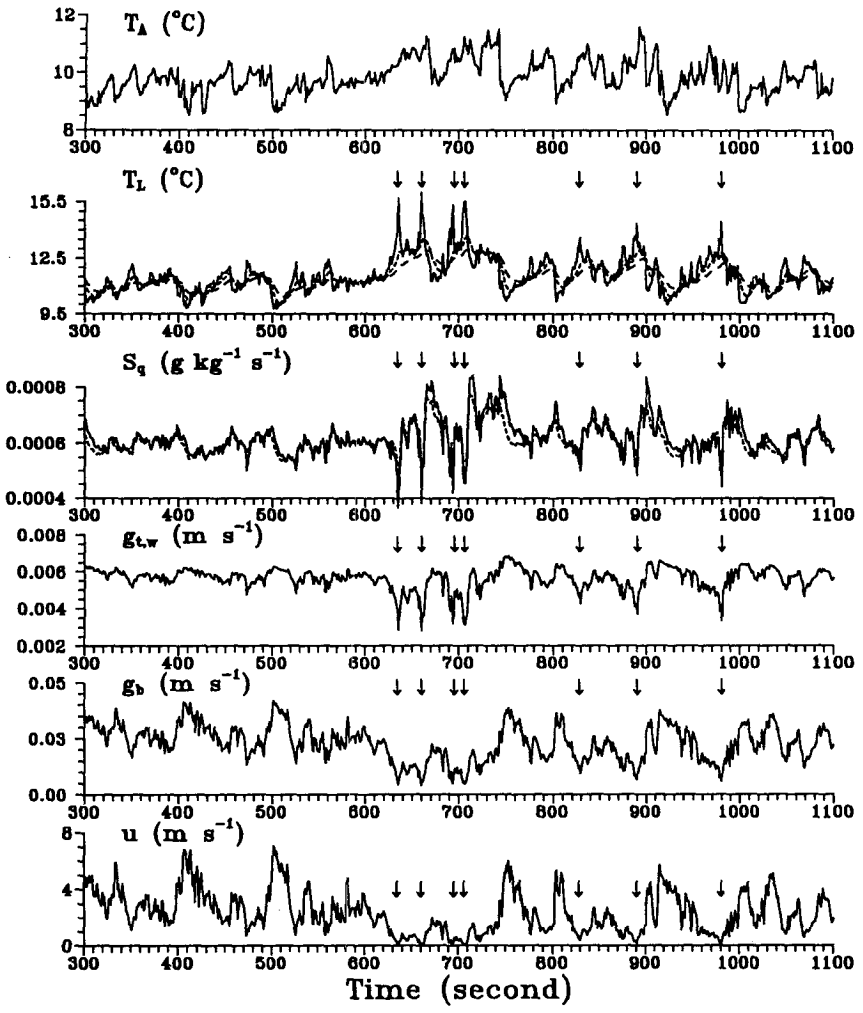

FIG. 10. Time series of air temperature T_A, leaf temperature T_L (solid line—no thermal storage; short dashed line—0.1-mm leaf; long dashed line—0.3-mm leaf), evaporation rate S_q (solid line—instant stomatal response; dashed line—20-s time lag added), total leaf conductance to water vapor $g_{t,w}$, leaf boundary layer conductance g_b, and wind speed u in the top layer of model forest.

leaf boundary layer conductance g_b varies as fast as the wind speed u (see Fig. 10) and is also one of the factors determining CO_2 assimilation rate S_C. However, as shown in section 4a, g_b is the dominant limit of CO_2 assimilation only when wind is very light. Otherwise, factors such as the PAR absorbed by plant leaves and

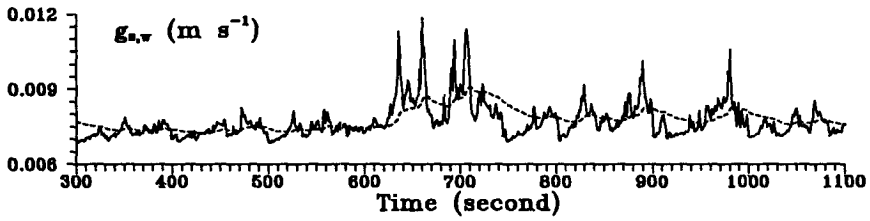

FIG. 11. Time series of leaf stomatal conductance to water vapor $g_{s,w}$ (solid line—instant response; dashed line—20-s time lag added) in the top layer of model forest.

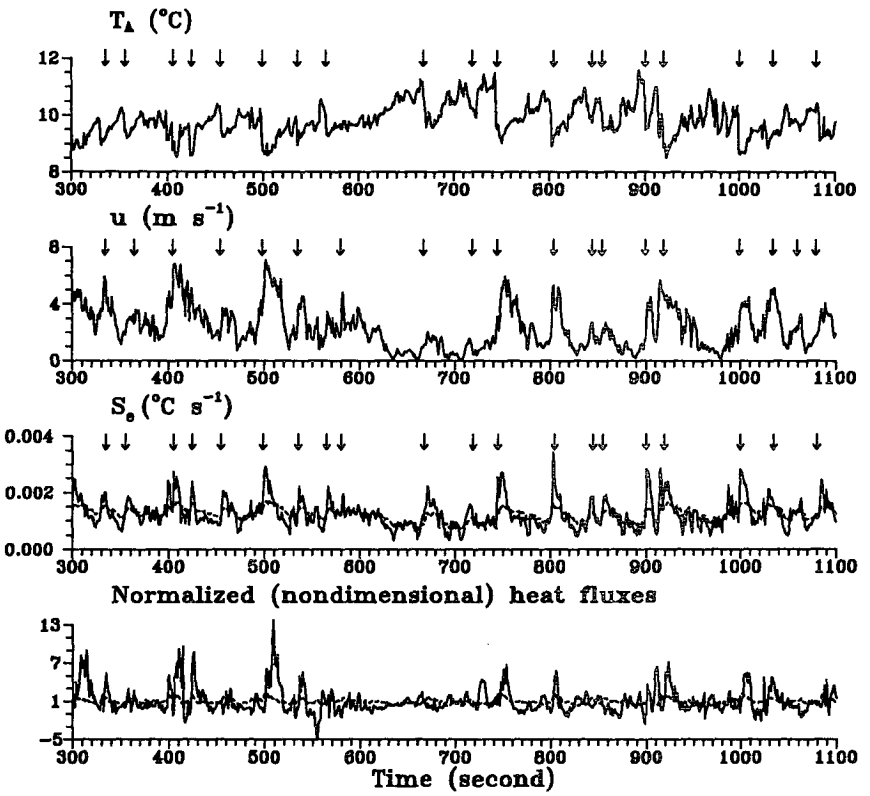

FIG. 12. Time series of air temperature T_A, wind speed u, subgrid volume-averaged rate of leaf–air exchange of sensible heat S_θ (solid line—thermal storage included; dashed line—thermal storage excluded), and normalized eddy-covariance heat flux $w'T'_A$ (solid line) and S_θ (dashed line) in the top layer of model forest.

the leaf temperature, which are either constant or vary relatively more slowly with time than do the wind speed u and the leaf boundary conductance g_b, are more important in determining the CO_2 assimilation rate S_C. For example, the absorbed PAR photon flux density was assumed to be constant during the 30-min period, and the leaf temperature varied much more smoothly than did the wind speed and the leaf boundary conductance g_b when the thermal storage was included (see Fig. 10).

6. Summary and conclusions

A single leaf model was developed by coupling a leaf energy balance equation with the Ball–Berry leaf stomatal conductance model, a biochemical photosynthesis model for C_3 species, and a canopy radiation model. A numerical iteration scheme was presented for solving this system by coupling an analytical solution for leaf stomatal conductance to water vapor $g_{s,w}$ to those for net CO_2 assimilation rate A_n and leaf temperature T_L. Sensitivity tests regarding the numerical behavior of the analytical solutions to leaf stomatal conductance $g_{s,w}$ and net CO_2 assimilation rate A_n in wide environmental conditions were also discussed.

A preliminary application of these coupled leaf and canopy models in modeling vertical variations of heating or cooling, evaporation, and CO_2 assimilation by leaves in each layer of a horizontally uniform forest canopy was performed for given environmental conditions. Modeled results are physically and physiologically reasonable.

The physical storage term was important in modeling transient leaf temperature and heating or cooling rate. An exponential formula was used to obtain realistic transient leaf stomatal conductance, which is important for estimation of transpiration rate. However, more appropriate time constants for stomatal opening and closing for different species are needed from experimental studies on stomatal behavior. In addition, the time interval of 1 s is sufficient to resolve the transiencies of both leaf temperature and stomatal conductance.

Other factors that have not been considered here might be important in a real environment within a plant canopy. For example, the Ball–Berry model does not

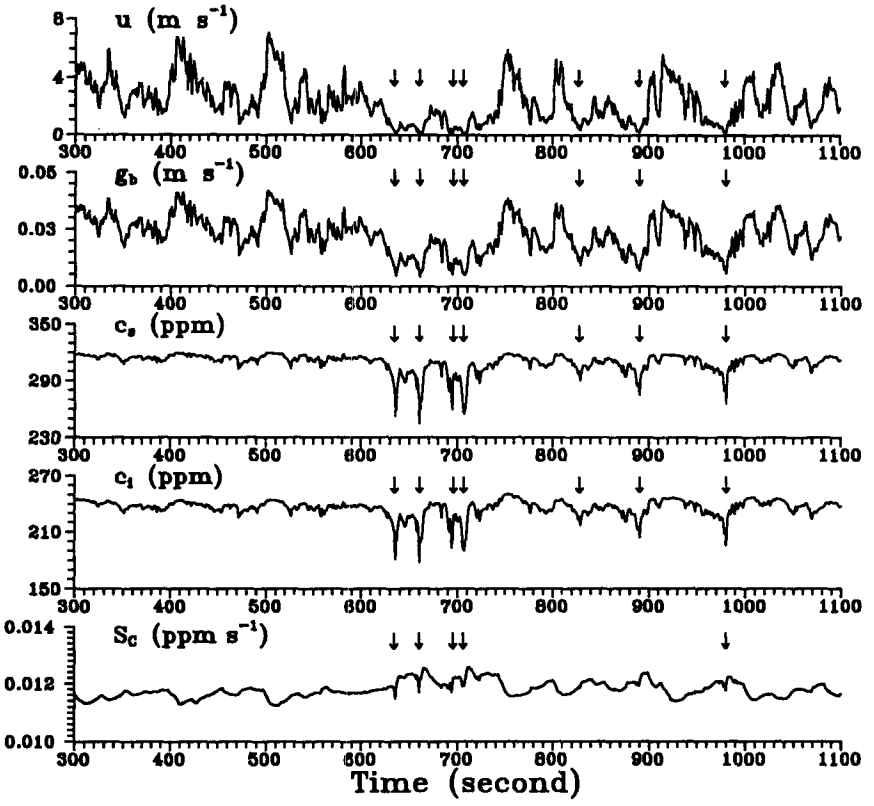

FIG. 13. Time series of wind speed u, leaf boundary layer conductance g_b, CO_2 concentration at the leaf surface c_s and in the intercellular space c_i, and subgrid volume-averaged CO_2 assimilation rate S_C in the top layer of model forest.

include effects of the water potential of leaves, branches, stems, and roots or soil water potential (Turner 1974; Jones 1992). Inclusion of such factors in the leaf stomatal conductance model is expected to improve the performance of our model when soil moisture is a limiting factor.

With regard to detailed verification and calibration of such models of plant–atmosphere interactions within a specific plant canopy, laboratory and field experiments are needed to obtain the empirical parameters used in the above stomatal conductance model and photosynthesis model for the particular plant species that constitute the plant canopy.

Acknowledgments. This work was partially supported by a National Science Foundation grant (ATM-92-16345) and a National Aeronautics and Space Administration project (SIR-C-029; Jet Propulsion Laboratory Contract 958445), and a Department of Energy program for ecosystem research project (DE-FGO3-93-ER-6187).

The authors greatly appreciate helpful discussions with Dr. Robert Pearcy. We also wish to thank two anonymous reviewers for their helpful comments.

APPENDIX

List of Abbreviations and Variables

A_E	RuBP regeneration limit of CO_2 assimilation (mol m^{-2} s^{-1})
a_L	leaf area density in each subgrid volume (m^{-1})
A_L	surface area of a single leaf (m^2)
A_n	net CO_2 assimilation rate at the leaf surface (mol m^{-2} s^{-1})
A_R	Rubisco activity limit of CO_2 assimilation (mol m^{-2} s^{-1})
b	intercept in the Ball–Berry leaf stomatal conductance model (mol m^{-2} s^{-1})
c_i	intercellular CO_2 concentration (ppm)
C_1, C_2 and C_3	empirical constants used in the leaf boundary layer conductance model
C_L	specific heat of leaf (J kg^{-1} K^{-1})
C_p	specific heat of air at constant pressure (J kg^{-1} K^{-1})
c_s	CO_2 concentration at leaf surface (ppm)
D_L	characteristic dimension of an individual leaf (m)

g gravitational acceleration (m s^{-2})
g_b leaf boundary layer conductance (m s^{-1} or mol m^{-2} s^{-1})
Gr Grashof number
$g_{s,w}$ leaf stomatal conductance to water vapor (mol m^{-2} s^{-1} or m s^{-1})
H sensible heat flux at the surface of a single leaf (W m^{-2})
IR infrared radiation (also called thermal or longwave radiation)
J potential rate of whole-chain electron transport rate (mol m^{-2} s^{-1})
J_{max} maximum rate of whole-chain electron transport at saturated light (mol m^{-2} s^{-1})
K_c Michaelis constant for CO_2 (mol mol^{-1})
K_o Michaelis constant for O_2 (mol mol^{-1})
LAI leaf area index of the whole canopy
LE latent heat flux at the surface of a single leaf (W m^{-2})
LES large-eddy simulation
L_v latent heat of vaporization (J kg^{-1})
m slope in the Ball–Berry leaf stomatal conductance model
NIR near-infrared radiation
Nu Nusselt number
o_i intercellular O_2 concentration (mol mol^{-1})
P total atmospheric pressure (Pa)
PAR photosynthetically active radiation
PFD photon flux density (mol m^{-2} s^{-1})
Q absorbed PAR photon flux density by a single leaf (mol m^{-2} s^{-1})
q_A water vapor mixing ratio in the air (g kg^{-1})
$q_s(T_L)$ saturated mixing ratio of water vapor at leaf temperature T_L (g kg^{-1})
$R_{a,l}$ absorbed longwave irradiance by a single leaf (W m^{-2})
$R_{a,s}$ absorbed total shortwave irradiance by a single leaf (W m^{-2})
R_d day respiration rate (mol m^{-2} s^{-1})
Re Reynolds number
$R_{e,l}$ emitted longwave irradiance by a single leaf (W m^{-2})
rh_s fractional relative humidity at leaf surface
RuBP ribulose bisphosphate
S thermal storage by a single leaf (W m^{-2})
S_C subgrid volume-averaged CO_2 assimilation rate by plant leaves (ppm s^{-1})
S_q subgrid volume-averaged evaporation rate from plant leaves (g kg^{-1} s^{-1})
S_θ subgrid volume-averaged heating or cooling rate by plant leaves (°C s^{-1})
T_L leaf temperature (°C)
T_A air temperature (°C)
V_c rate of carboxylation (mol m^{-2} s^{-1})
V_{cmax} maximum catalytic activity of Rubisco at saturated RuBP and CO_2 (mol m^{-2} s^{-1})
V_L volume of a single leaf (m^3)
V_o rate of oxygenation (mol m^{-2} s^{-1})
u wind speed (m s^{-1})
α quantum efficiency
β_θ volumetric expansion coefficient of air (K^{-1})
$\gamma_{w,c}$ ratio of molecular diffusivity of water vapor to that of CO_2
Γ_* CO_2 compensation point (ppm)
ϵ_L thermal emissivity of leaf
θ curvature factor for solving the whole chain electron transport rate J
ν kinematic molecular diffusivity of air (m^2 s^{-1})
ν_θ thermal molecular diffusivity of air (m^2 s^{-1})
ρ air density (kg m^{-3})
ρ_L leaf density (kg m^{-3})
σ Stefan–Boltzmann constant (W m^{-2} K^{-4})
τ_s time constant of leaf stomatal opening and closing (s)

REFERENCES

Baldocchi, D., 1994a: An analytical solution for coupled leaf photosynthesis and stomatal conductance models. *Tree Physiol.*, **14,** 1069–1079.

——, 1994b: Are crops and forest spherical? The role of canopy radiative transfer models on calculating canopy CO_2 and energy exchange rates. *21st Conf. on Agricultural and Forest Meteorology,* San Diego, CA, Amer. Meteor. Soc., 9–11.

Ball, J. T., 1988: An analysis of stomatal conductance. Ph.D. thesis, Stanford University, 89 pp.

——, and J. A. Berry, 1982: The c_i/c_s ratio: A basis for predicting stomatal control of photosynthesis. *Carnegie Inst. Washington, Year Book.* **81,** 88–92.

Brooks, A., and G. D. Farquhar, 1985: Effect of temperature on the CO_2/O_2 specificity of ribulose-1, 5-bisphosphate carboxylase/oxygenase and the rate of respiration in the light. *Planta,* **165,** 397–406.

Denmead, O. T., and E. F. Bradley, 1985: Flux-gradient relationships in a forest canopy. *The Forest–Atmosphere Interaction,* B. A. Hutchison and B. B. Hicks, Eds., D. Reidel Publishing Co., 421–442.

Evans, J. R., and G. D. Farquhar, 1991: Modeling canopy photosynthesis from the biochemistry of the C_3 chloroplast. *Modeling Crop Photosynthesis—From Biochemistry to Canopy,* K. J. Boote and R. S. Loomis, Eds., Crop Science Society of America, Inc. and American Society of Agronomy, Inc., 140 pp.

Fanjul, L., and H. G. Jones, 1982: Rapid stomatal responses to humidity. *Planta,* **154,** 135–138.

Farquhar, G. D., 1988: Models relating subcellular effects of temperature to whole plant responses. *Plants and Temperature,* S. P. Long and F. I. Woodward, Eds., The Company of Biologists Limited, 395–409.

——, and S. von Caemmerer, 1982: Modelling of photosynthetic response to environmental conditions. *Encyclopedia of Plant Physiology,* 12B, O. L. Lange, P. S. Nobel, C. B. Osmond, and H. Ziegler, Eds., Springer-Verlag, 549–588.

——, ——, and J. A. Berry, 1980: A biochemical model of photosynthetic CO_2 assimilation in leaves of C_3 species. *Planta,* **149,** 78–90.

Gao, W., Shaw, R. H., and K. T. Paw U, 1989: Observation of organized structure in turbulent flow within and above a forest canopy. *Bound.-Layer Meteor.,* **47,** 349–377.

Jones, H. G., 1992: *Plants and Microclimate, A Quantitative Approach to Environmental Plant Physiology.* 2d ed. Cambridge University Press, 428 pp.

Kaimal, J. C., and J. J. Finnigan, 1994: *Atmospheric Boundary Layer Flows.* Oxford University Press, 289 pp.

Kirschbaum, M. U. F., and G. D. Farquhar, 1984: Temperature dependence of whole-leaf photosynthesis in Eucalyptus pauciflora Sieb. ex Spreng. *Aust. J. Plant Physiol.,* **11,** 519–538.

Leuning, R., 1990: Modelling stomatal behavior and photosynthesis of *Eucalyptus grandis. Aust. J. Plant Physiol.,* **17,** 159–175.

Meyers, T. P., and K. T. Paw U, 1987: Modelling the plant canopy micrometeorology with higher-order closure principles. *Agric. For. Meteor.,* **41,** 143–163.

Monteith, J. L., 1973: *Principles of Environmental Physics.* Edward Arnold Limited, 241 pp.

Norman, J. M., 1979: Modeling the complete crop canopy. *Modification of the Aerial Environment of Crops,* B. J. Barfield and J. F. Gerber, Eds., American Society of Agricultural Engineers, 538 pp.

Patton, E. G., R. H. Shaw, and K. T. Paw U, 1995: Large-eddy simulation of a forest: Influence of canopy structure on turbulent kinetic energy. Preprints, *11th Symp. on Boundary Layers and Turbulence,* Charlotte, NC, Amer. Meteor. Soc., 525–528.

Paw U, K. T., 1987: Mathematical analysis of the operative temperature and energy budget. *J. Therm. Biol.,* **12,** 227–233.

——, and T. P. Meyers, 1989: Investigations with a higher-order canopy turbulence model into mean source-sink levels and bulk canopy resistances. *Agric. For. Meteor.,* **47,** 259–271.

——, Y. Brunet, S. Collineau, R. H. Shaw, T. Maitani, J. Qiu, and L. Hipps, 1992: On coherent structures in turbulence above and within agricultural plant canopies. *Agric. For. Meteor.,* **61,** 55–68.

Shaw, R. H., and U. Schumann, 1992: Large-eddy simulation of turbulent flow above and within a forest. *Bound.-Layer Meteor.,* **61,** 47–64.

——, G. Den Hartog, and H. H. Neumann, 1988: Influence of foliar density and thermal stability on profiles of Reynolds stress and turbulence intensity in a deciduous forest. *Bound.-Layer Meteor.,* **45,** 391–409.

——, K. T. Paw U, and W. Gao, 1989: Detection of temperature ramps and flow structure at a deciduous forest site. *Agric. For. Meteor.,* **47,** 123–138.

Turner, N. C., 1974: Stomatal behavior and water status of maize, sorghum and tobacco under field conditions. *Plant Physiol.,* **53,** 360–365.

Weiss, A., and J. M. Norman, 1985: Partitioning solar radiation into direct and diffuse, visible and near-infrared components. *Agric. For. Meteor.,* **34,** 205–213.

Wong, S. C., I. R. Cowan, and G. D. Farquhar, 1979: Stomatal conductance correlates with photosynthesis capacity. *Nature,* **282,** 424–426.